nature communications

Article

https://doi.org/10.1038/s41467-024-55511-4

Chemical looping synthesis of amines from N_2 via iron nitride as a mediator

Received: 24 June 2024

Accepted: 12 December 2024

Published online: 02 January 2025

Check for updates

Haoyue Li[1,2], Tie Wang[1,2], Shifu Wang[3], Xuning Li[3], Yanqiang Huang[3] & Ning Yan[1,2,4]

Amines are commonly synthesized through the amination of organooxygenates using ammonia, frequently involving the use of noble metal catalysts. In this study, we present an alternative route to make amines using iron nitride ($Fe_{2.5}N$) as the nitrogen source. Without any additional catalyst, $Fe_{2.5}N$ reacts with a range of alcohols at 250 °C under 1 or 10 bar H_2 to produce amines as major products. Mechanistic investigations indicate that hydrogen activates the nitrogen species within iron nitride, converting them into surface NH and NH_2 groups that then react with alcohols to form amines. Building on this foundation, we further demonstrate an iron nitride-mediated chemical looping pathway that utilizes N_2 as the nitrogen source to synthesize octylamines. In this process, N_2 first reacts with iron to form Fe_xN by a ball-milling method at ambient temperature and 6 bar N_2. The as-prepared Fe_xN subsequently reacts with alcohols to yield amines, transferring over 80% of the nitrogen to organic compounds. This looping process proves stable across four cycles.

Nitrogen-containing chemicals, particularly amines, are key building blocks for chemical industries[1–10]. Currently, the primary nitrogen source for synthesizing these compounds, ammonia, is produced from the Haber-Bosch process—the single most energy-intensive processes globally operating at 400–500 °C and 200–250 bar[11,12]. Additionally, amination reactions using ammonia often require noble metal catalysts because many substrates do not efficiently react with ammonia. Even with catalysts, the single-pass conversion of NH_3 remains low, typically ranging from 0.2-7% (Fig. 1 and Supplementary Table 1). Given these challenges, there has been a sustained effort to develop alternative pathways that enable the production of nitrogen-containing organic compounds starting from N_2, bypassing the Haber-Bosch process.

Exciting progresses have been made in the synthesis of organonitrogen chemicals directly from N_2, primarily utilizing Li in metallic or other highly reactive states (Supplementary Table 2). For instance, Li has been employed as the reductant for the synthesis of N_2-transition metal complexes as key intermediates[13] or for the direct conversion of N_2 to organonitrogen chemicals[14]. Li also reacts with N_2 to form Li_3N, which further interacts with reactive species such as aromatic halides or aromatic acyl chlorides to construct C–N bonds[15]. Additionally, key synthons like Li_2CN_2 have been synthesized from LiH and N_2, serving as precursors for accessing organonitrogen chemicals[16]. Despite these elegant studies, the high redox potential of Li makes the preparation and regeneration of metallic Li energy-intensive[15], and its high reactivity also necessitates precautions in wide application. Beyond Li, organometallic complexes of Mo and Ti have also been explored, showing potential in activating N_2[17–19] and leading to the formation of organonitrogen chemicals in the presence of Pd catalysts[20,21].

Nevertheless, no studies have yet harnessed inexpensive 3-d metals as effective mediators to synthesize organonitrogen chemicals from N_2. We propose that 3-d metal nitrides could serve as promising candidates to bridge N_2 to organonitrogen compounds. Investigations into the release of nitrogen atoms from 3-d transition metal nitrides under H_2[22–25], CO[26], and mixed atmosphere of CO_2 and H_2[27], have shown that lattice nitrogen is labile and reactive, potentially facilitating C–N bond formation. Furthermore, a range of 3-d metals, including Ti[28], Cr[29], Mn[30,31], and Fe[32] have reacted with N_2 to form metal

[1]Joint School of National University of Singapore and Tianjin University, International Campus of Tianjin University, Binhai New City, Fuzhou, China. [2]Department of Chemical and Biomolecular Engineering, National University of Singapore, Singapore, Singapore. [3]State Key Laboratory of Catalysis, Dalian Institute of Chemical Physics, Chinese Academy of Sciences, Dalian, China. [4]Centre for Hydrogen Innovations, National University of Singapore, Singapore, Singapore. e-mail: ning.yan@nus.edu.sg

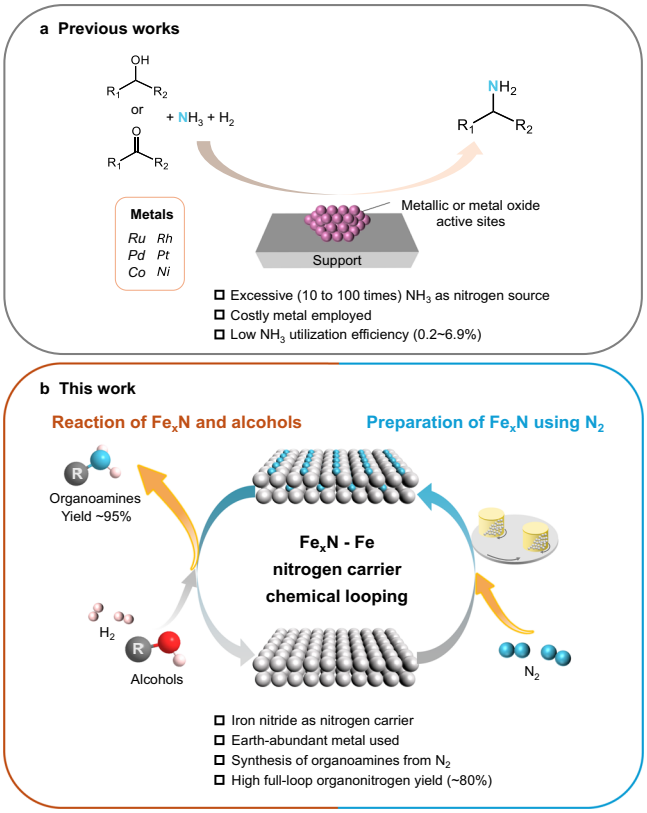

Fig. 1 | Comparison between previous amine production and proposed N_2-to-amine production. a Catalytic amination of alcohols/aldehydes using NH_3. **b** The proposed Fe_xN-mediated chemical looping pathway to synthesize organoamines. (Left) Organoamines synthesis using Fe_xN, (Right) Preparation of stable Fe_xN using N_2.

nitrides[33,34]. With a moderate nitrogen binding energy that enables both the fixation of N_2 to nitride, as well as the transfer of nitrogen in the nitride into organonitrogen chemicals, 3-d transition metal nitrides may thus serve as effective nitrogen carriers[35].

In this study, we report our advances in the chemical looping synthesis of organonitrogen compounds using iron nitride as the nitrogen carrier (Fig. 1). We first investigated the reactivity of iron nitride ($Fe_{2.5}N$) in converting isopropanol to isopropylamine and di-isopropylamine, demonstrating that iron nitride is a superior nitrogen source for amine synthesis compared to ammonia (Fig. 1b, left). We then expanded our investigation to include a range of alcohols—primary, secondary, and tertiary—to broaden the applicability of this method. Finally, we demonstrated the effectiveness of the N_2-nitridated iron powder (Fe_xN), made at ambient temperature and low pressure, as a nitrogen source for amine synthesis, during which itself is converted back to metallic iron. Through these efforts, we establish a cheap 3 d metal-based chemical looping process for organonitrogen synthesis beginning with N_2 (Fig. 1b).

Results

Synthesis and reactivity of $Fe_{2.5}N$

We initially prepared iron nitride with stoichiometric Fe:N ratio (2.5:1, terms as $Fe_{2.5}N$)[36] for reactivity study, while the more challenging synthesis of Fe_xN from N_2 and metallic iron was explored later. The fresh $Fe_{2.5}N$ sample exhibited aggregates of 100 nm-1μm particles with irregular shapes (Fig. 2a, Supplementary Fig. 1a–e, and Supplementary Fig. 2a–f) and small surface area (14 $m^2 \cdot g^{-1}$, Supplementary Table 3). The XRD pattern of the sample matches that of Fe_2N (PDF #73-2102) and Fe_3N phase (PDF #72-2125) (Fig. 2c). The lattice fringe spacing (d value) was 0.210 nm, 0.239 nm, and 0.302 nm, corresponding to the (-1 -1 1), (1 1 0), and (1 0 1) crystal plane of ε-phase[37] Fe_2N/Fe_3N hexagonal structure, respectively (Fig. 2a and Supplementary Fig. 2). The N content of was 9.1 wt.% (Supplementary Table 4), confirming a Fe:N ratio of ~2.5:1. In the Mössbauer spectra (Fig. 2e), a doublet peak corresponding to ε-$Fe_{2.1}N$ is the major phase while a low-intensity sextet corresponding to γ-Fe_4N coexists (Supplementary Table 5)[38,39]. In the XPS spectra (Fig. 2d and Supplementary Fig. 3), the peaks at around 397.6 eV, 396.7 eV, and 399.1 eV corresponded to Fe-O-N, Fe-N and adsorbed NH_3, respectively (Supplementary Fig. 4 and Table 6)[40–42]. The adsorption edge of the fresh $Fe_{2.5}N$ in the XANES spectrum (Fig. 2f) was in between the reference Fe foil and FeO. Fourier transform of Fe K-edge EXAFS of the $Fe_{2.5}N$ was also performed: the peaks centered at ~1.56 Å and ~2.27 Å correspond to Fe-N and Fe-Fe shells, respectively[43,44], consistent with the interstitial structure of iron nitride. $Fe_{2.5}N$ was thermally stable under inert atmosphere below 400 °C, after which it decomposes, releasing N_2 (Supplementary Fig. 5).

Next, the amination of isopropanol was conducted in a continuous fixed-bed reactor, with $Fe_{2.5}N$ placed inside the reactor while a mixture of H_2 and Ar carried isopropanol vapor through the sample bed (Fig. 3a). The study focuses on the conversion of nitrogen in $Fe_{2.5}N$, so that the product yields were calculated on nitrogen basis. $Fe_{2.5}N$ was inactive at 150 °C, but notable productivity towards amines, including isopropylamine and di-isopropylamine, was observed at 200 °C. The best performance was achieved at 250 °C, resulting in a high organonitrogen selectivity of 23% under 5 bar H_2 (Fig. 3b). At this temperature, the conversion of isopropanol remained relatively stable in the first 5 h (Supplementary Fig. 6), while the yield of organonitrogen compounds gradually decreased, indicating the nitrogen consumption led to the decrease amine production. Hydrocarbons and oxygenates (C_6-C_9) were the major non-nitrogen-containing products (Supplementary Fig. 7–8). When the temperature further increased to 300 °C, the most favorable reaction became hydrodeoxygenation.

At optimum temperature (250 °C), the variation of H_2 partial pressure from 0 to 10 bar significantly influenced amine formation (Fig. 3c). Without H_2, only a minor fraction of organonitrogen compounds were formed, likely through the hydrogen-borrowing pathway as observed in catalytic amination of alcohols[45–47]. Increasing the hydrogen partial pressure to 1 bar substantially enhanced amine production. Further increasing the H_2 partial pressure led to reduced amine yields, attributable to the enhanced formation of ammonia, thereby limiting the nitrogen available to form the organonitrogen products. Additionally, H_2 is known to hinder the dehydrogenation of isopropanol[48–51].

The consumption of nitrogen in $Fe_{2.5}N$ at optimal condition over time is illustrated in Fig. 3d. The 5 hours of reaction at 250 °C with 1 bar H_2 led to almost total loss of nitrogen, where 37% of the initial nitrogen had been transformed into amines, and the remaining amount was present as gaseous NH_3. The nitrogen balance of the system was also monitored in 2 h and 5 h reactions and both results were close to 100%, indicating a well-balanced reaction system (Supplementary Fig. 9). After 32-hour reaction (Supplementary Table 4), N was completely depleted. The data indicate a positive correlation between the amination rate and the nitrogen content in $Fe_{2.5}N$.

The spent $Fe_{2.5}N$ remained similar shape (Fig. 2b, Supplementary Fig. 1f–j, and Supplementary Fig. 2g–k) and surface area (12 $m^2 \cdot g^{-1}$, Supplementary Table 3) compared with fresh $Fe_{2.5}N$. The lattice fringe spacing of 32-hour spent $Fe_{2.5}N$ corresponds to the (1 1 0) crystal plane of metallic iron, and the XRD patterns of both 2-hour and 32-hour spent $Fe_{2.5}N$ also corresponded well with metallic Fe phase (Fig. 2c). For the 2 h and 32 h spent $Fe_{2.5}N$, the Mössbauer spectrum showed only the sextet corresponding to α-Fe[38,52]. In XPS analysis, the presence of N could still be observed in the 2-hour spent $Fe_{2.5}N$ (Fig. 2d and Supplementary Fig. 3), but no nitrogen was seen in the 32-hour spent $Fe_{2.5}N$. These results consistently suggest that the lattice nitrogen in $Fe_{2.5}N$ was gradually consumed during the reaction while Fe species are transformed into metallic Fe.

https://doi.org/10.1038/s41467-024-55511-4

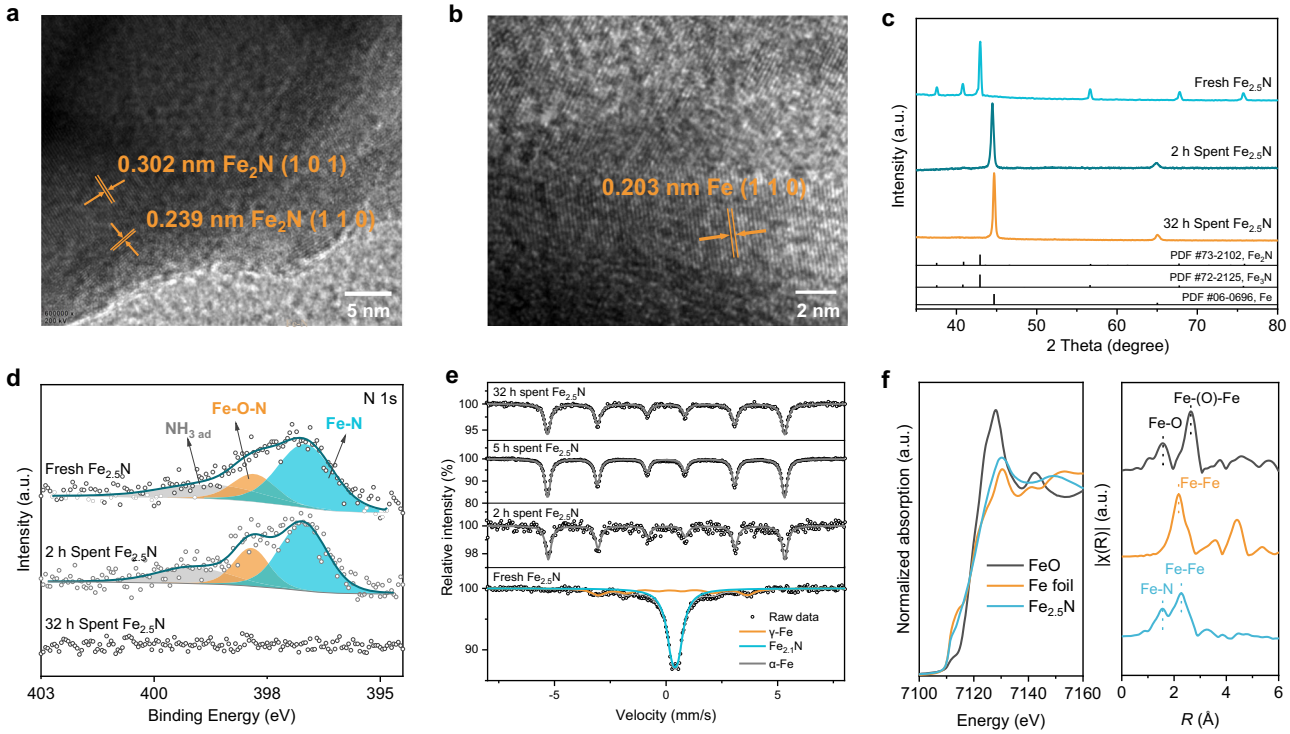

Fig. 2 | Identifying nitrogen existence and phase transition of $Fe_{2.5}N$ during reaction. HR-TEM image of fresh (**a**) $Fe_{2.5}N$ and (**b**) spent $Fe_{2.5}N$ (32 h reaction), (**c**) XRD patterns and (**d**) XPS high-resolution N 1 s spectra of the fresh $Fe_{2.5}N$, 2 h spent, 5 h spent, and 32 h spent $Fe_{2.5}N$, (**e**) ^{57}Fe-Mössbauer spectra of fresh, 2 h spent, 5 h spent and 32 h spent $Fe_{2.5}N$ obtained at 298 K (**f**) Fe K-edge XANES spectra and FT-EXAFS spectra of fresh $Fe_{2.5}N$, reference FeO, and reference Fe foil.

Reaction mechanism and substrate scope

Figure 4a displays the in-situ DRIFTS spectra of isopropanol adsorption on fresh $Fe_{2.5}N$ under H_2 atmosphere at 250 °C. The peak at 3656 cm^{-1} is attributed to the O-H stretching of isopropanol[53]. More importantly, the peak at 2655 cm^{-1} corresponds to the characteristic peak of isopropylamine (Supplementary Fig. 10), indicating the formation of the desired product. The peak at 1738 cm^{-1} is assigned to C=O stretching[54,55], revealing the presence of acetone[56]. The peaks at 1651 and 1642 cm^{-1} are ascribed to C=N stretching[57], and the peak at 1246 cm^{-1} arises from C-N stretching[58,59]. Vibrations of NH_x species bonded to Fe sites are also observed[27]. Further assignments of peaks are provided in the supporting information (Supplementary Table 7). Using ammonia as a probe molecule, Lewis acid sites was identified on $Fe_{2.5}N$ (Supplementary Fig. 11)[54,60,61], which are known to be beneficial for dehydrogenation of alcohol[62], activation of C=O[63,64], and hydrogenation of C=N[63].

Acetone was further employed as a substrate to react with $Fe_{2.5}N$ (Fig. 4b). At both 200 °C and 250 °C, acetone generated the same types of products as isopropanol did, such as isopropylamine, di-isopropylamine, and Schiff base (Supplementary Fig. 8), demonstrating that acetone is a viable intermediate for amine formation. The concurrent formation of isopropanol could possibly be from the hydrogenation of acetone catalyzed by iron nitride which is known to be active in hydrogenation reactions[27]. Compared to using alcohol, the production of amine compounds is much more prominent at a lower 200 °C, indicating that the dehydrogenation of isopropanol to acetone is likely to be rate-limiting.

The reduction behavior of $Fe_{2.5}N$ was investigated under H_2 (Fig. 4c). A prominent peak, identified as NH_3, appeared at 520 °C, demonstrating the transformation of lattice nitrogen in $Fe_{2.5}N$ to form NH_3. The NH_3 signal below 335 °C was minimal, supporting the notion that the chosen amination reaction temperature of 250 °C reduced the undesirable side reaction of producing ammonia.

We propose the following mechanism for the reaction (Fig. 4d). Initially, isopropanol is adsorbed on the Lewis acid sites of the iron nitride and undergoes dehydrogenation to yield acetone. Subsequently, the NH_x present on $Fe_{2.5}N$ surface transforms acetone into imine, which is then hydrogenated to isopropylamine. As surface nitrogen is progressively consumed, the lattice nitrogen migrates to the surface for further amination, during which $Fe_{2.5}N$ is gradually converted to metallic iron. This reaction pathway is analogous to the conventional amination mechanism, but the nitrogen source is lattice nitrogen. Given that hydrogen also reacts with $Fe_{2.5}N$ to produce ammonia, the existence of a conventional amination pathway cannot be entirely excluded.

To validate the wide applicability of amine production using iron nitride as the nitrogen source, we evaluated the reaction between $Fe_{2.5}N$ and a range of alcohols in a batch reactor. The findings revealed that primary alcohols (Fig. 5) react more effectively than secondary alcohols, while tertiary alcohols show no reactivity in forming amines. This variation in reactivity is attributed to the steric hindrance in secondary alcohols and the absence of α-H in tertiary alcohols, which prevents the formation of the crucial C=O intermediate. Additionally, primary alcohols exhibited a higher selectivity for producing tertiary amines, likely due to the greater stability of tertiary amines. The highest amine yield achieved is 95.2% with 1-decanol as substrate. These results suggest that $Fe_{2.5}N$ has broad applicability and adaptability across different alcohol substrates and add supporting evidence for the proposed mechanism of alcohol dehydrogenation followed by solid N (in $Fe_{2.5}N$)-dominated amination.

N_2-to-amine via Fe_xN as a mediator

To enable an iron nitride-mediated looping pathway to make amines using N_2 as nitrogen source, we synthesized iron nitride from N_2 following an elegant recent report based on a mechanochemical approach[65]. Typically, iron powder was loaded into ball-mill jar with iron

https://doi.org/10.1038/s41467-024-55511-4

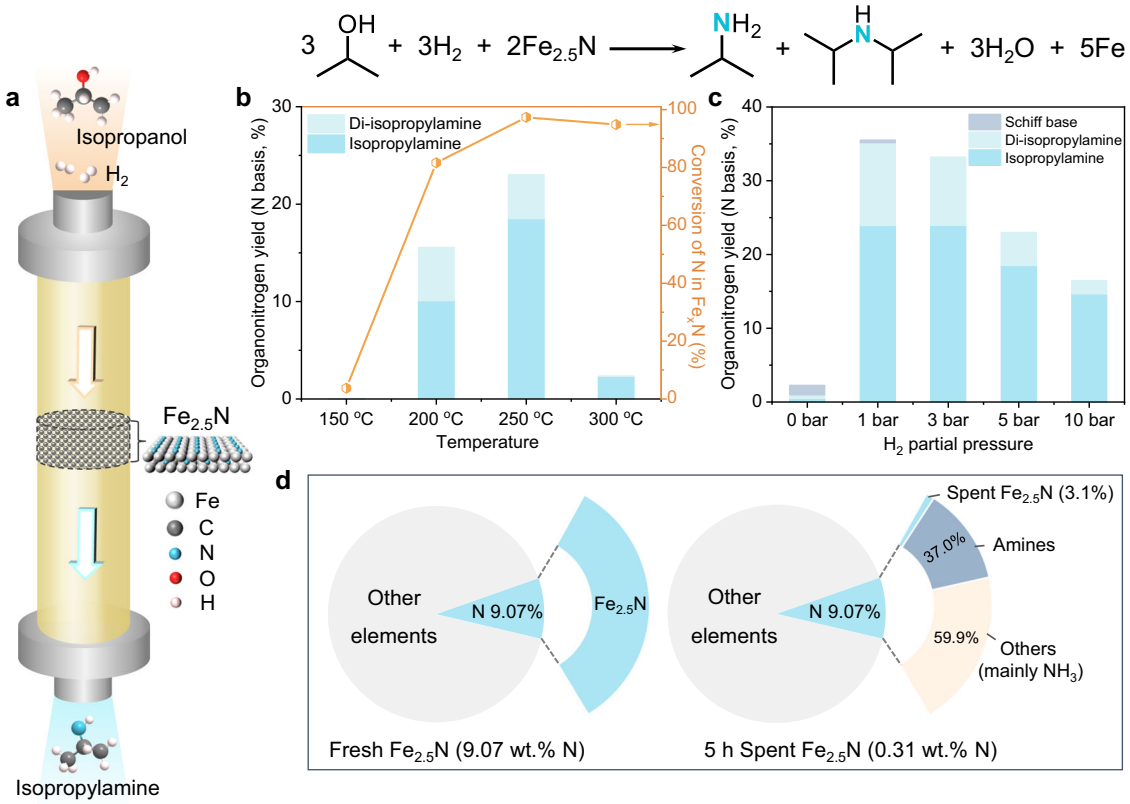

Fig. 3 | Reaction performance of $Fe_{2.5}N$ with isopropanol under H_2. a Reaction set-up. **b** Organonitrogen yield (5 h) and conversion of N in $Fe_{2.5}N$ at different temperatures with 5 bar H_2. Organonitrogen yield = $n_{Organonitrogen}/n_{N_{fresh}}$. Conversion of N in $Fe_{2.5}N = (n_{N_{fresh}} - n_{N_{spent}})/n_{N_{fresh}}$. Total flow rate: 60 mL/min, total pressure: 10 bar. isopropanol supplying rate: $1.438*10^{-5}$ mol/min. **c** Organonitrogen yield (5 h) at 250 °C with different H_2 partial pressures. **d** N content and conversion of N in $Fe_{2.5}N$ (fresh and 5 h spent), 5 h spent $Fe_{2.5}N$ was obtained after the reaction at 250 °C with 1 bar H_2 (optimal condition).

balls and charged with 6 bar of N_2 for the ball milling to synthesize iron nitride (Fe_xN) without heat supply. N 1 s XPS spectra of the as-prepared Fe_xN clearly showed the existence of N on the surface (Fig. 6a). The XRD patterns of the as-prepared Fe_xN and commercial iron powder are shown in Fig. 6b. A peak shift towards lower angle caused by N insertion is observed after ball milling under N_2 atmosphere. The presence of N in the as-prepared Fe_xN was further ambiguously confirmed by EDX mapping of SEM and TEM (Supplementary Fig. 12 and Table 8) and CHN elemental analysis (Supplementary Table 4). Based on the acid treatment method (Supplementary Table 9), the N content in the as-prepared Fe_xN was 0.4 wt.%.

The as-prepared Fe_xN was subsequently reacted with octanol in the same manner as described in the previous session. Encouragingly, around 80% N in the as-prepared Fe_xN was transferred to octylamines, majority of which was trioctylamine due to its higher stability. Post-reaction Fe_xN was washed with methanol and freeze-dried before taking to the next round looping synthesis. The nitrogen content of the spent Fe_xN was not detected by acid treatment and elemental analysis, (Supplementary Tables 4 and 9) indicating the N in Fe_xN was depleted during the reaction. The excellent activity maintained throughout the 4 cycles, highlighting the high N utilization efficiency and durability of the proposed N_2-to-amine looping strategy. The overall activity and specific selectivity towards dioctylamine both increased with increasing cycles, which could be explained by enriched H species on the iron nitride surface during repeated use, which facilitates reaction and product desorption.

Discussion

In conclusion, this study provides an entry point into the broader potential for transition metal nitrides as the nitrogen carrier bridging the looping synthesis of organonitrogen chemicals from N_2. We confirmed the donation of nitrogen from iron nitride to alcohols, with the concurrent transformation of Fe species metal nitride into metallic Fe. When $Fe_{2.5}N$ was used as a nitrogen carrier, more than 85% of the nitrogen was extracted to produce amines from C_6-C_{10} primary alcohols in a batch reactor at 250 °C and 10 bar H_2. More importantly, Fe_xN, produced by nitridating iron powder with N_2 at ambient temperature and low pressure, has proven to be an effective nitrogen source for the catalyst-free production of organic amines. High N utilization efficiency of over 80% was consistently achieved over 4 cycles. To enhance its applicability, additional efforts should focus on increasing the nitrogen content of Fe_xN, such as by nanostructuring of Fe or alloying it with a second metal. Despite this, our study unlocks the previously untapped potential of using inexpensive 3d-transition metal nitrides to produce organonitrogen compounds with N_2 as the nitrogen source.

Methods

Materials

2-propanol (≥99.5%) and phenol (99%) were purchased from Fisher Scientific Pte. Ltd. Iron (≥99%, reduced, fine powder), concentrated sulfuric acid (ACS reagent, 95.0–98.0%), concentrated hydrochloric acid (ACS reagent, 37%), potassium hydroxide (ACS reagent, ≥85%, pellets), isopropylamine (≥99.5%), acetone (anhydrous, ≥99.5%), cyclohexanol (99%), 1-butanol (99.8%), 1-hexanol (≥99%), 1-octanol (≥99%), 1-decanol (98%), and tert-butanol (≥99.5%) were provided by Sigma-Aldrich Pte. Ltd. (Singapore). Fe_3O_4 (≥97%) was purchased from Shanghai Macklin Biochemical Co., Ltd.

https://doi.org/10.1038/s41467-024-55511-4

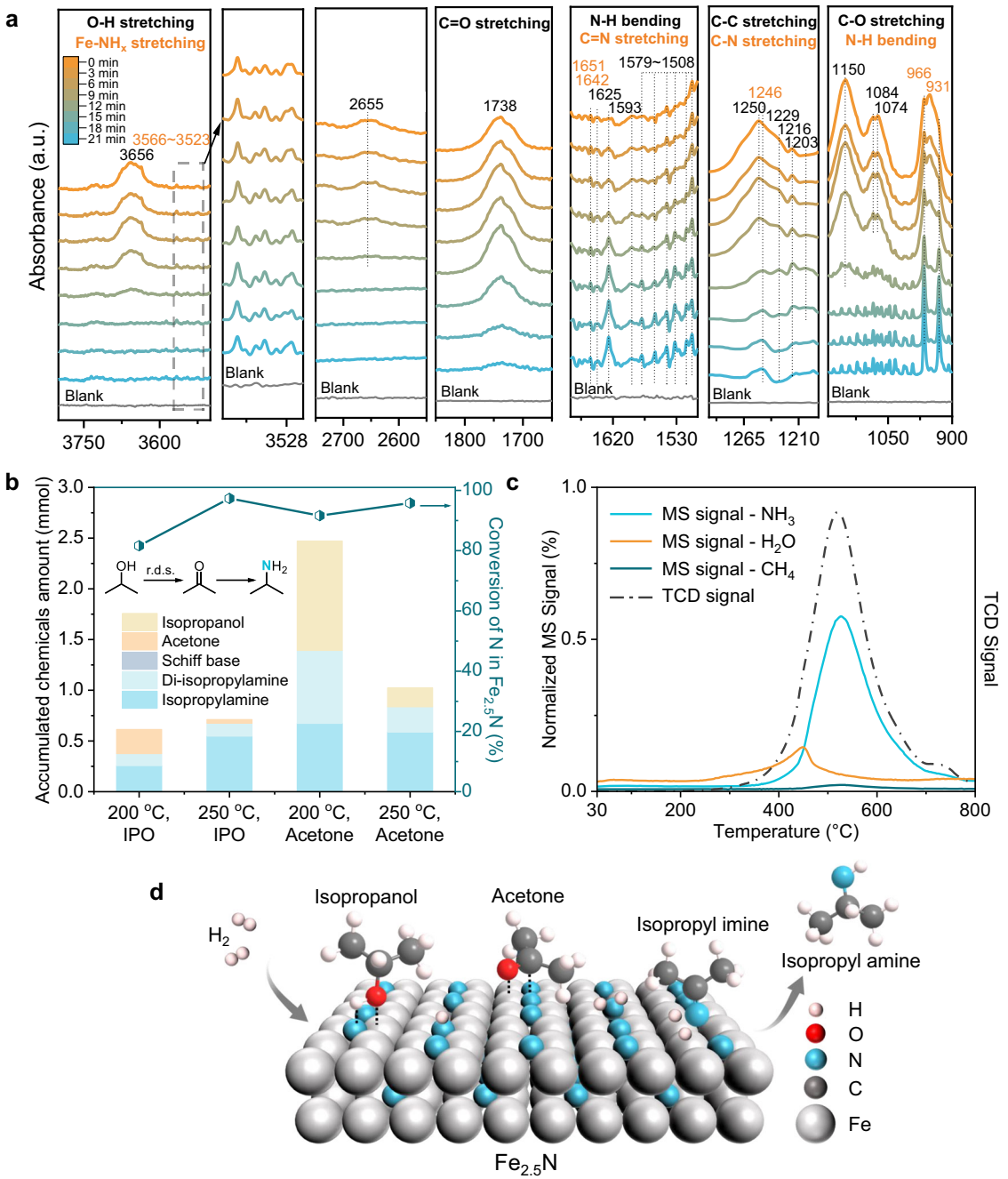

Fig. 4 | Probing reaction mechanism of amine production over $Fe_{2.5}N$. a DRIFTS spectra of $Fe_{2.5}N$ after isopropanol adsorption. **b** Conversion of isopropanol or acetone to isopropylamine at different temperatures with 5 bar H_2. Reaction time: 5 h. Conversion of N in $Fe_{2.5}N = (n_{N_{fresh}} - n_{N_{spent}})/n_{N_{fresh}}$. Total flow rate: 60 mL/min; the total pressure: 10 bar. isopropanol supplying rate: $1.438*10^{-5}$ mol/min. **c** H_2-TPR profile and MS signals of $Fe_{2.5}N$ under 5% H_2/N_2 (NH_3 MS signal: m/z = 17). **d** The proposed reaction mechanism.

Typical activity test

The catalytic performance tests were carried out in a vertical, fixed-bed tube reactor (SS316), with a reactor tube length of 0.5 m and a diameter of 7.6 mm. A furnace (1.2 kW, 220 V, up to 1000 °C) was utilized to heat the reactor, and a thermocouple was inserted into the catalyst bed to monitor the temperature in real-time. The temperature was regulated by a temperature controller that was inserted into the reactor. The samples were diluted with quartz sand and held in place with quartz wool to form a sample bed in the middle of the reactor. The liquid substrates were first introduced into a three-way autoclave, which had dedicated paths for the addition of liquid substrates, a gas supply, and a gas outlet connected to the reactor tube. The autoclave was maintained in the water bath at 25 °C, and the pressure inside was regulated using a back pressure valve. The gas inlet path of the autoclave was submerged at the bottom of the liquid for bubbling so that the liquid-vapor could be carried by the gas to enter the reactor and go through the sample bed, while the hydrogen gas and argon gas were supplied to the autoclave controlled by gas flow meters.

Iron nitride ($Fe_{2.5}N$) was prepared by nitridating commercial Fe_3O_4 under 40 mL/min atmospheric NH_3 at 600 °C for 120 min. After nitridation, the $Fe_{2.5}N$ was purged in Ar at 40 mL/min after cooling down to 300 °C to purge out residue NH_3 while avoiding $Fe_{2.5}N$ decomposition. Characterizations were conducted after

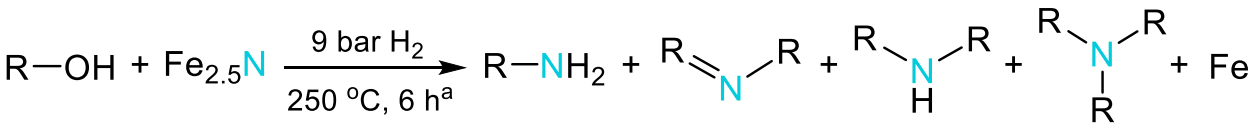

R = ^{n}Bu-, ^{n}Hex-, ^{n}Oct, ^{n}Dec-, ^{i}Pr-, Cyc-, etc.

[a]Reaction conditions: 1 mL substrate, 50 mg $Fe_{2.5}N$, 9 bar H_2, 250 °C, 6 h.
[b]Organonitrogen yield [%] = the amount of organonitrogen products (mol) / the amount of input N in $Fe_{2.5}N$ (mol).
[c]Organonitrogen products total amount.
[d]N.D. stands for "not detected".

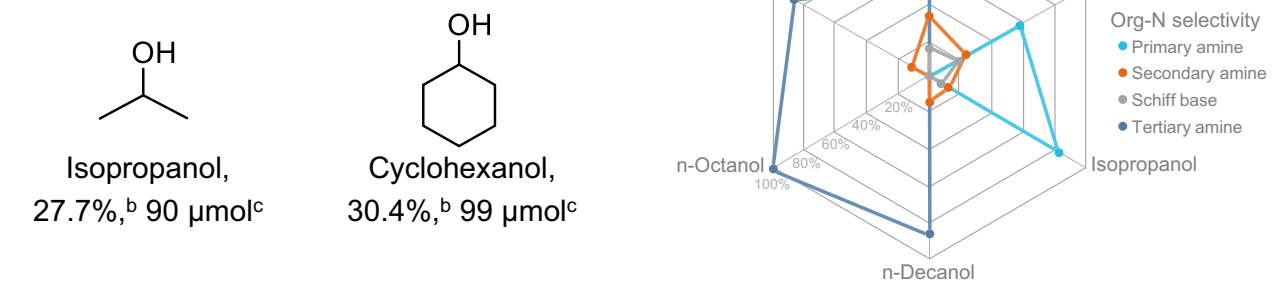

Isopropanol, 27.7%,[b] 90 μmol[c]

Cyclohexanol, 30.4%,[b] 99 μmol[c]

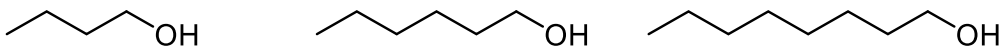

n-Butanol, 48.7%,[b] 158 μmol[c]

n-Hexanol, 89.0%,[b] 289 μmol[c]

n-Octanol, 87.5%,[b] 284 μmol[c]

n-Decanol, 95.2%,[b] 309 μmol[c]

t-Butanol, N.D.[d]

Phenol, N.D.[d]

Fig. 5 | The extraction of N in $Fe_{2.5}N$ with different alcohols. Top: The chemical equation representing proposed transformation. **Bottom:** Alcohols tested accompanied with corresponding yields (below each molecule) and the selectivity towards primary, secondary, tertiary amine, and Schiff base summarized in the radar chart.

combining $Fe_{2.5}N$ samples obtained in multiple nitridation batches. For each reaction test, 0.5 g of $Fe_{2.5}N$ was loaded in the fixed bed flow reactor. After loading $Fe_{2.5}N$ in the middle of the reactor and increasing the temperature to the reaction temperature (250 °C for a typical test) under Ar, substrates mixed with H_2 and Ar were supplied into the reactor at desired flow rates with a fixed total gas flow of 60 mL/min. The mean gas residence time is 22.7 s during the typical activity test in the fixed-bed flow reactor. Since $Fe_{2.5}N$ was prepared, all the storage and loading were conducted in glovebox with ultra-dry apparatus as water contamination could be detrimental to the amine production performance (Supplementary Table 10). The products were collected and analyzed by an online GC-FID system equipped with an Agilent CAM capillary column. The outlet flow could also be collected by passing through a bottle of methanol in the ice bath to obtain the organic chemicals for off-line GC or GC-MS analysis.

Activity test for substrate scope (Autoclave batch reactor)

The transformation of alcohols with $Fe_{2.5}N$ was also performed in an autoclave. For example, 50 mg $Fe_{2.5}N$, 70 μL dodecane (internal standard), and 1 mL alcohol substrates were added to the reactor in the glovebox. After that, the autoclave was introduced with 9 bar H_2, and placed in a metal jacket wafer on an electronic hotplate (typically 250 °C). After 6 hours of reaction, the reactor was immediately terminated by cooling the reactor in ice. The gas phase products were collected by gas bag, and the gas was then bubbled into the diluted sulfuric acid solution. The obtained solution was detected by IC (ion chromatography). The liquid products were collected and tested by GC and GC-MS for qualification and quantification analysis.

The synthesis and activity test of N_2-nitridated Fe (Fe_xN)

Specifically, iron powder (5 g) and iron balls (50 g, 5 mm diameter) were loaded into the ball-mill jar (50 mL) inside an Ar-atmosphere

https://doi.org/10.1038/s41467-024-55511-4

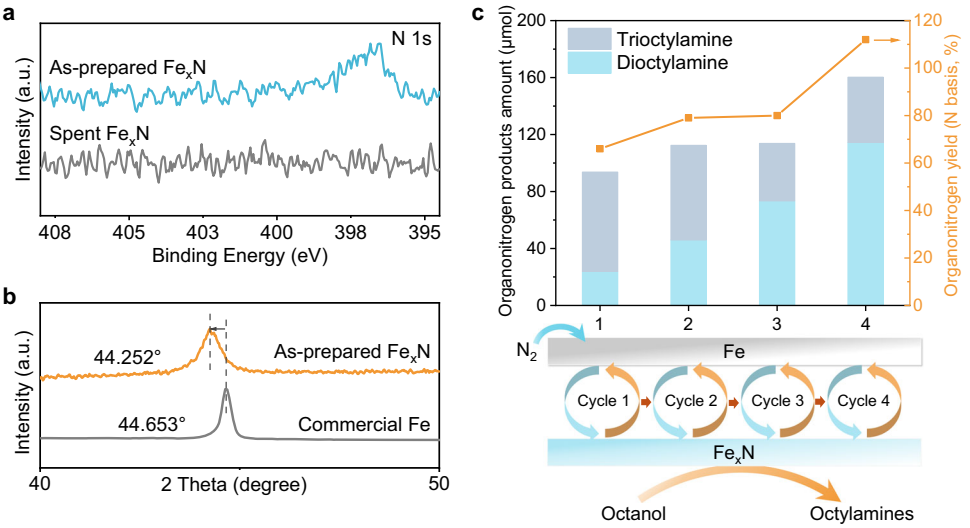

Fig. 6 | The chemical looping synthesis of octylamines from N_2 with Fe_xN as nitrogen carrier. a XPS spectra of as-prepared Fe_xN and spent Fe_xN, **b** XRD patterns of as-prepared Fe_xN and commercial Fe, **c** Organonitrogen products amount and organonitrogen yield (N basis) within 4 cycles of the N_2-to-amines synthesis system. The as-prepared Fe_xN was prepared by ball milling in N_2 (6 bar) at rotation speed of 2000 r.p.m. for 30 h. Octylamine production reaction condition: 1 mL octanol, 5 g Fe_xN, 10 bar H_2, 250 °C, 6 h. Organonitrogen yield [%] = the number of organonitrogen products / the amount of input N in Fe_xN.

glovebox. The ball-mill jar was then evacuated and charged to 6 bar using N_2 before being taken to the planetary ball mill machine for 30 h 2000 rpm ball milling. The ball milling was stopped for 10 min every 30 min to release the heat.

The as-prepared Fe_xN powder was transferred into an autoclave, together with 1 mL octanol and 70 μL dodecane (internal standard). The autoclave was purged with 10 bar H_2 more than 10 times carefully to exchange the Ar inside. After purging, the batch reactor was charged with 10 bar H_2, and reacted at 250 °C for 6 h on an electronic hotplate with metal jacket. Similarly, the reactor was instantly cooled with ice after 6 hours of reaction, and the gas phase was carefully released into a 0.5 M sulfuric acid solution. The liquid products were washed with 1 mL methanol and tested by GC-FID and GC-MS. The remaining spent Fe_xN powder was further washed with 50 mL methanol 3 times inside the glovebox before being taken to ball-mill reaction with nitrogen gas again.

N content determination

The nitrogen content of iron nitride samples was determined by dissolving 0.1 g of the sample in 30 mL 0.2 M hydrochloric acid at 80 °C overnight. After that, 50 mL of 5 M KOH solution was injected to the clear aliquot under continuous N_2 purging at 80 °C. The outlet gas was bubbled through 10 mL of 0.5 M sulfuric acid for 2 hours, which was taken to IC analysis for NH_4^+ concentration.

Characterization

The crystal structure of iron nitride was tested by a Bruker D8 Advance X-Ray diffractometer, equipped with a Cu Kα source (40 kV, 30 mA). BET surface areas were calculated from nitrogen adsorption isotherms obtained by N_2 adsorption and desorption at 77 K in a Micromeritics ASAP 2020 surface area. Scanning electron microscopy (SEM) was performed with a JEOL JSM-7610F. Transmission electron microscopy images were acquired on a JEM 2100 F (JEOL, Japan) microscope operated at 200 kV. XPS spectra were recorded on a VG Escalab MKII spectrometer, using a mono Al Kα X-ray source (hv = 1486.71 eV, 5 mA, 15 kV), and the calibration was done by setting the C1s peak at 284.5 eV. Elemental mappings of iron nitride were obtained using an JEOL microscope equipped with a Bruker Quantax energy-dispersive X-ray spectrometer (EDXS). CHN elemental analysis was conducted on the Thermo Scientific Flashsmart CHNS analyzer. The room temperature ^{57}Fe Mössbauer spectrum was observed on a Topologic 500 A spectrometer, which equipped ^{57}Co(Rh) as the radioactive source. Fitted by the MössWinn 4.0, all of the spectra were distinguished by different parameters, such as quadrupole splitting (QS) and isomer shift (IS). Besides, an α-iron foil was used to calibrate the IS values and Doppler velocities.

In situ diffuse reflectance infrared Fourier transform (DRIFT) spectra were acquired on a Thermo Scientific Nicolet iS50 FT-IR. The measurement was under atmospheric pressure, with ZnSe window and MCT-A detector cooled by liquid nitrogen. The solid Fe_3O_4 powder was treated at 550 °C under 30 mL/min NH_3 flow for 30 minutes in the cell to in situ form iron nitride, and then the temperature was changed to the required temperature under the H_2 flow or the Ar flow for the in-situ observation. The background was recorded under Ar before testing samples. The vapor of the liquid substrate was carried by the Ar gas flow into the cell. The NH_3 gas was supplied by the gas sample bag injection and degassed under Ar gas flow. The spectra were recorded with 4 cm^{-1} resolution of 32 scans.

H_2-TPR-MS measurements were performed using a Quantachrome instrument coupled with a quadrupole mass spectrometer (Hidden Analytical). Prior to the measurements, the sample was pretreated in a flow of pure He gas at 150 °C to remove the moisture and any contaminants. The H_2-TPR profile was obtained by heating the sample from 30 °C to 800 °C at the rate of 10 °C/min in a 5% H_2/N_2 atmosphere, while Ar-TPD (decomposition) measurements were conducted under pure Ar flow when heating the sample at the rate of 10 °C/min to 800 °C. The mass spectrometer was set to record the gas outlet composition.

Ex situ Fe K-edge XAS measurements were conducted at a public beamline, BL01B1, Spring-8 (Japan Synchrotron Radiation Research Institute, Hyogo, Japan). (Proposal Number: 2023A1533) The incident X-rays were monochromatized with a Si (111) double crystal monochromator. Conventional Fe K-edge XAS spectra of a Fe metal foil, FeO, Fe_3O_4, and Fe_2O_3 were collected as reference data. Data were reduced using the Athena and Artemis software ver. 0.9.26 included in the Demeter package. The 7 mm catalyst pellets were made from a thoroughly ground mixture of 1.1 mg Fe_xN with 60 mg boron nitride.

Data availability

The authors declare that the data supporting the findings of this study are available within the paper and its Supplementary Information file. Should any raw data files be needed in another format they are available from the corresponding author upon request.

References

1. Stankiewicz, B. A. & Van Bergen, P. F. In Nitrogen-containing macromolecules in the bio- and geosphere Vol. 707 *ACS Symposium Series* Ch. 1, 1–12 (American Chemical Society, 1998).
2. Hitosugi, T. et al. Tyrosine phosphorylation inhibits PKM2 to promote the Warburg effect and tumor growth. *Sci.Signal.* **2**, ra73 (2009).
3. Yu, J., Shi, F. & Gong, L. Brønsted-acid-catalyzed asymmetric multicomponent reactions for the facile synthesis of highly enantioenriched structurally diverse nitrogenous heterocycles. *Acc. Chem. Res.* **44**, 1156–1171 (2011).
4. Lang, K. D., Kaur, R., Arora, R., Saini, B. & Arora, S. Nitrogen-containing heterocycles as anticancer agents: An overview. *Anticancer Agents Med. Chem.* **20**, 2150–2168 (2020).
5. Heravi, M. M. & Zadsirjan, V. Prescribed drugs containing nitrogen heterocycles: An overview. *RSC Adv.* **10**, 44247–44311 (2020).
6. Meier, M. A. R. Plant-oil-based polyamides and polyurethanes: Toward sustainable nitrogen-containing thermoplastic materials. *Macromol. Rapid Commun.* **40**, 1800524 (2019).
7. Stejskal, J., Sapurina, I. & Trchová, M. Polyaniline nanostructures and the role of aniline oligomers in their formation. *Prog. Polym. Sci.* **35**, 1420–1481 (2010).
8. Noro, S.-I., Kitagawa, S., Akutagawa, T. & Nakamura, T. Coordination polymers constructed from transition metal ions and organic N-containing heterocyclic ligands: Crystal structures and microporous properties. *Prog. Polym. Sci.* **34**, 240–279 (2009).
9. Kong, Q., Wei, J., Hu, Y. & Wei, C. Fabrication of terminal amino hyperbranched polymer modified graphene oxide and its prominent adsorption performance towards Cr(VI). *J. Hazard. Mater.* **363**, 161–169 (2019).
10. Wang, J., Deng, B., Chen, H., Wang, X. & Zheng, J. Removal of aqueous Hg(II) by polyaniline: Sorption characteristics and mechanisms. *Environ. Sci. Technol.* **43**, 5223–5228 (2009).
11. Chen, X., Song, S., Li, H., Gözaydın, G. & Yan, N. Expanding the boundary of biorefinery: Organonitrogen chemicals from biomass. *Acc. Chem. Res.* **54**, 1711–1722 (2021).
12. Zhao, Y. et al. Layered-double-hydroxide nanosheets as efficient visible-light-driven photocatalysts for dinitrogen fixation. *Adv. Mater.* **29**, 1703828 (2017).
13. Wang, K. et al. Synthesis of arylamines and N-heterocycles by direct catalytic nitrogenation using N_2. *Nat. Commun.* **12**, 248 (2021).
14. Lv, Z.-J. et al. Direct transformation of dinitrogen: synthesis of N-containing organic compounds via N-C bond formation. *Natl. Sci. Rev.* **7**, 1564–1583 (2020).
15. Chen, G.-F. et al. Saving the energy loss in Lithium-mediated nitrogen fixation by using a highly reactive Li_3N intermediate for C –N coupling reactions. *Angew. Chem. Int. Ed.* **61**, e202203170 (2022).
16. Shi, X. et al. Synthesis of pyrimidines from dinitrogen and carbon. *Natl. Sci. Rev.* **9**, nwac168 (2022).
17. Volpin, M. E., Shur, V. B., Kudryavtsev, R. V. & Prodayko, L. A. Amine formation in molecular nitrogen fixation: nitrogen insertion into transition metal–carbon bonds. *Chem. Commun*. 1038–1040 (1968).
18. Keane, A. J., Farrell, W. S., Yonke, B. L., Zavalij, P. Y. & Sita, L. R. Metal-mediated production of isocyanates, $R_3EN{=}C{=}O$ from dinitrogen, carbon dioxide, and R_3ECl. *Angew. Chem. Int. Ed.* **54**, 10220–10224 (2015).
19. Curley, J. J., Sceats, E. L. & Cummins, C. C. A cycle for organic nitrile synthesis via dinitrogen cleavage. *J. Am. Chem. Soc.* **128**, 14036–14037 (2006).
20. Hori, K. & Mori, M. Synthesis of nonsubstituted anilines from molecular nitrogen via transmetalation of arylpalladium complex with Titanium–Nitrogen fixation complexes. *J. Am. Chem. Soc.* **120**, 7651–7652 (1998).
21. Ueda, K., Sato, Y. & Mori, M. Incorporation of N_2 and CO into organic molecules: Amide formation by Palladium-catalyzed carbonylation and nitrogenation. *J. Am. Chem. Soc.* **122**, 10722–10723 (2000).
22. Tricker, A. W. et al. Mechanocatalytic ammonia synthesis over TiN in transient microenvironments. *ACS Energy Lett.* **5**, 3362–3367 (2020).
23. Wang, S. et al. Transition metal enhanced chromium nitride as composite nitrogen carrier for sustainable chemical looping ammonia synthesis. *Appl. Catal. B.* **339**, 123134 (2023).
24. Yang, S. et al. Molybdenum-based nitrogen carrier for ammonia production via a chemical looping route. *Appl. Catal. B.* **312**, 121404 (2022).
25. Wang, B., Yin, X., Wang, P. & Shen, L. Chemical looping ammonia synthesis at atmospheric pressure benefiting from synergistic effect of Mn- and Fe-based nitrogen carriers. *Int. J. Hydrogen Energy* **48**, 2705–2717 (2023).
26. Goodeve, C. & Jack, K. H. Kinetics of nitrogen evolution from an iron-nitrogen interstitial alloy. *Discuss. Faraday Soc.* **4**, 82–91 (1948).
27. Zhao, B. et al. Unveiling the activity origin of iron nitride as a catalytic material for efficient hydrogenation of CO_2 to C_{2+} hydrocarbons. *Angew. Chem. Int. Ed.* **60**, 4496–4500 (2021).
28. Hlavacek, V. Combustion synthesis: A historical perspective. *Am. Ceram. Soc. Bull.* **70**, 240–243 (1991).
29. Lyutaya, M. D. & Kulik, O. P. Some characteristics of the formation of chromium nitrides. *Powder Metall. Met. Ceram.* **13**, 792–794 (1974).
30. Lyutaya, M. D. & Goncharuk, A. B. Manganese nitrides. *Powder Metall. Met. Ceram.* **16**, 208–212 (1977).
31. Mohammadi Aframehr, W. & Pfromm, P. H. Activating dinitrogen for chemical looping ammonia synthesis: Nitridation of manganese. *J. Mater. Sci.* **56**, 12584–12595 (2021).
32. Gray, H. H. & Thompson, M. B. The action of molecular nitrogen on highly purified iron. *J. Phys. Chem.* **36**, 889–908 (1932).
33. Zong, F. et al. Synthesis and characterization of magnesium nitride powder formed by Mg direct reaction with N_2. *J. Alloys Compd.* **508**, 172–176 (2010).
34. Rabenau, A. & Schulz, H. Re-evaluation of the lithium nitride structure. *J. Less-Common Met.* **50**, 155–159 (1976).
35. Jacobsen, C. J. H. et al. Catalyst design by interpolation in the periodic table: Bimetallic ammonia synthesis catalysts. *J. Am. Chem. Soc.* **123**, 8404–8405 (2001).
36. Zhang, H. et al. Implication of iron nitride species to enhance the catalytic activity and stability of carbon nanotubes supported Fe catalysts for carbon-free hydrogen production via low-temperature ammonia decomposition. *Catal. Sci. Technol.* **8**, 907–915 (2018).
37. Jack, K. H. The iron–nitrogen system: the crystal structures of ε-phase iron nitrides. *Acta Crystallogr* **5**, 404–411 (1952).
38. Prieto, P., Marco, J. F. & Sanz, J. M. Synthesis and characterization of iron nitrides. An XRD, Mössbauer, RBS and XPS characterization. *Surf. Interface Anal.* **40**, 781–785 (2008).
39. Brumovsky, M. et al. Iron nitride nanoparticles for enhanced reductive dechlorination of trichloroethylene. *Environ. Sci. Technol.* **56**, 4425–4436 (2022).
40. Bouanis, F. Z., Jama, C., Traisnel, M. & Bentiss, F. Study of corrosion resistance properties of nitrided carbon steel using radiofrequency N_2/H_2 cold plasma process. *Corros. Sci.* **52**, 3180–3190 (2010).
41. Kumaresan, L., Shanmugavelayutham, G. & Saravanan, P. Single-phase ferromagnetic iron nitride (ε-Fe_3N) nanoparticles synthesized

by thermal plasma method for oxygen evolution and supercapacitor applications. *Appl. Phys. A* **128**, 1073 (2022).
42. Bhattacharyya, S., Shivaprasad, S. M. & Gajbhiye, N. S. Variation of magnetic ordering in ε-Fe_3N nanoparticles. *Chem. Phys. Lett.* **496**, 122–127 (2010).
43. Pee-Yew, L., Chung-Kwei, L., Chieh-Lung, C., Yeukuang, H. & Tsung-Shune, C. In *1999 IEEE International Magnetics Conference (INTERMAG)*. DP13-DP13 (IEEE).
44. Okudera, H. et al. Local structure of magnetite and maghemite and chemical shift in Fe K-edge XANES. *J. Mineral. Petrol. Sci.* **107**, 127–132 (2012).
45. Irrgang, T. & Kempe, R. 3d-Metal catalyzed N- and C-alkylation reactions via borrowing hydrogen or hydrogen autotransfer. *Chem. Rev.* **119**, 2524–2549 (2019).
46. Bähn, S. et al. The catalytic amination of alcohols. *ChemCatChem* **3**, 1853–1864 (2011).
47. Jagadeesh, R. V. et al. MOF-derived cobalt nanoparticles catalyze a general synthesis of amines. *Science* **358**, 326–332 (2017).
48. Wang, Y. et al. Catalytic production of alanine from waste glycerol. *Angew. Chem. Int. Ed.* **59**, 2289–2293 (2020).
49. Wang, T. et al. Rational design of selective metal catalysts for alcohol amination with ammonia. *Nat. Catal.* **2**, 773–779 (2019).
50. Kita, Y., Kuwabara, M., Yamadera, S., Kamata, K. & Hara, M. Effects of ruthenium hydride species on primary amine synthesis by direct amination of alcohols over a heterogeneous Ru catalyst. *Chem. Sci.* **11**, 9884–9890 (2020).
51. Li, S. et al. Amination of isopropanol to isopropylamine over a highly basic and active Ni/LaAlSiO catalyst. *J. Catal.* **350**, 141–148 (2017).
52. Smirnov, G. V., Van Bürck, U., Chumakov, A. I., Baron, A. Q. R. & Rüffer, R. Synchrotron Mössbauer source. *Phys. Rev. B* **55**, 5811–5815 (1997).
53. Xu, W., Raftery, D. & Francisco, J. S. Effect of irradiation sources and oxygen concentration on the photocatalytic oxidation of 2-propanol and acetone studied by in situ FTIR. *J. Phys. Chem. B* **107**, 4537–4544 (2003).
54. Araña, J. et al. FTIR study of photocatalytic degradation of 2-propanol in gas phase with different TiO_2 catalysts. *Appl. Catal. B.* **89**, 204–213 (2009).
55. Gu, Q. et al. Photocatalytic reforming of C3-polyols for H_2 production: Part II. FTIR study on the adsorption and photocatalytic reforming reaction of 2-propanol on Pt/TiO_2. *Appl. Catal. B.* **106**, 689–696 (2011).
56. Martin, C., Martin, I., Rives, V., Grzybowska, B. & Gressel, I. A FTIR spectroscopy study of isopropanol reactivity on alkali-metal-doped MoO_3/TiO_2 catalysts. *Spectrochim. Acta A Mol. Biomol. Spectrosc.* **52**, 733–740 (1996).
57. Sotowa, K.-I., Amamoto, T., Sobana, A., Kusakabe, K. & Imato, T. Effect of treatment temperature on the amination of chlorinated diamond. *Diam. Relat. Mater.* **13**, 145–150 (2004).
58. Wilfong, W. C., Srikanth, C. S. & Chuang, S. S. In situ ATR and DRIFTS studies of the nature of adsorbed CO_2 on tetraethylenepentamine films. *ACS Appl. Mater. Interfaces* **6**, 13617–13626 (2014).
59. Maiyalagan, T. & Viswanathan, B. Template synthesis and characterization of well-aligned nitrogen containing carbon nanotubes. *Mater. Chem. Phys.* **93**, 291–295 (2005).
60. Chen, L., Si, Z., Wu, X. & Weng, D. DRIFT study of CuO-CeO_2-TiO_2 mixed oxides for NO_x reduction with NH_3 at low temperatures. *ACS Appl. Mater. Interfaces* **6**, 8134–8145 (2014).
61. Guntida, A., Suriye, K., Panpranot, J. & Praserthdam, P. Comparative study of Lewis acid transformation on non-reducible and reducible oxides under hydrogen atmosphere by in situ DRIFTS of adsorbed NH_3. *Top. Catal.* **61**, 1641–1652 (2018).
62. Tong, T. et al. Dual functions of CoO_x decoration in PtCo/CeO_2 catalysts for the hydrogen-borrowing amination of alcohols to primary amines. *J. Catal.* **378**, 392–401 (2019).
63. Nakamura, Y., Kon, K., Touchy, A. S., Shimizu, K.-I. & Ueda, W. Selective synthesis of primary amines by reductive amination of ketones with ammonia over supported Pt catalysts. *ChemCatChem* **7**, 921–924 (2015).
64. Liang, G. et al. Production of primary amines by reductive amination of biomass-derived aldehydes/ketones. *Angew. Chem. Int. Ed.* **56**, 3050–3054 (2017).
65. Han, G.-F. et al. Mechanochemistry for ammonia synthesis under mild conditions. *Nat. Nanotechnol.* **16**, 325–330 (2021).

Acknowledgements

We thank the NRF Investigatorship (NRF-NRFI07–2021–0006) for the financial support.

Author contributions

N.Y., H.Y.L., and T.W. designed the study. H.Y.L. and T.W. performed the experiments and interpreted the data. S.F.W., X.N.L., and Y.Q.H. conducted the Mössbauer experiments and processed the data collected. H.Y.L. and T.W. drafted the manuscript. N.Y., H.Y.L., T.W., S.F.W., X.N.L., and Y.Q.H. reviewed and revised the manuscript.

Competing interests

The authors declare no competing interests.

Additional information

Supplementary information The online version contains supplementary material available at https://doi.org/10.1038/s41467-024-55511-4.

Correspondence and requests for materials should be addressed to Ning Yan.

Peer review information *Nature Communications* thanks the anonymous reviewers for their contribution to the peer review of this work. A peer review file is available.